Journal of Energy Storage 53 (2022) 105181

Contents lists available at ScienceDirect

Journal of Energy Storage

journal homepage: www.elsevier.com/locate/est

Research papers

Dynamic response of hybrid energy storage based virtual inertial support in wind application

Nor Shahida Hasan [a,b,*], Norzanah Rosmin [a,b], Norjulia Mohamad Nordin [c], Saifulnizam Abd Bakar [c], Azana Hafizah Mohd Aman [d]

[a] Communication and Network Research Group, Malaysia-Japan International Institute of Technology, Universiti Teknologi Malaysia, 54100 Kuala Lumpur, Malaysia
[b] Centre of Electrical Energy Systems (CEES), School of Electrical Engineering, Faculty of Engineering, Universiti Teknologi Malaysia, 81310 Johor Bahru, Johor, Malaysia
[c] School of Electrical Engineeting, Faculty of Engineering, Universiti Teknologi Malaysia, 81310 Johor Bahru, Johor, Malaysia
[d] Faculty of Information Science and Technology, Universiti Kebangsaan Malaysia, 43600 UKM Bangi, Selangor, Malaysia

ARTICLE INFO

Keywords:
Wind system
Virtual energy storage
Hybrid energy storage
Energy storage management
Frequency nadir

ABSTRACT

The replacement of conventional synchronous generator (SG) with wind energy conversion system (WECS) greatly reduces the available inertial support in the electrical network. In order to avoid mechanical stress on wind turbine (WT) which is caused by kinetic energy (KE) extraction in providing the virtual inertial support (VIS), this paper proposed an improved technique in converting a hybrid energy storage (HES) into VIS during disturbances for wind turbine systems. The complementary behaviour of supercapacitor (SC) and battery energy storage (BES) offers a great deal of faster and limitless VIS. The trade-off between SC and BES has been achieved through a modified formulation of total available inertial time constant for HES-based VIS. To realize this, the new SC's voltage and BES's voltage are kept updated before being used to form the SC's and BES's reference current in the proposed model. Alongside in operating the HES-based VIS, this paper also introduced a modified energy management system (EMS) by fully utilizing the advantages of the high-power density of SC and the high-energy density of BES in handling disturbances. This modified control technique greatly provides faster and continuous VIS throughout the disturbances compared to the sole energy storage of SC and BES. In addition, based on the tested system of fixed wind speed and variable loads, the proposed HES-based VIS significantly improved the frequency nadir and peak frequency by 3.5 % and 2.7 % respectively. Additionally, the proposed HES-based VIS shows a significant improvement during variable wind speed and load conditions.

1. Introduction

1.1. General background

The global cumulative installed capacity of onshore wind power will be increased up to 5044 GW by 2050 compared to only 542 GW in 2018 [1]. However, frequency stability issues which are caused by the lack of inertial support in wind connected grid systems are quite concerning. Previously, this inertial support was supplied by a conventional Synchronous Generator (SG). As the high penetration Wind Energy Conversion Systems (WECS) take over the grid systems, the available inertial support which is required during power imbalances between supply and demand is gradually reduced. Practically, the wind systems did not have any ability to directly respond towards inertial response [2]. Therefore, additional supplementary control systems are required to extract the Virtual Inertial Support (VIS) during any disturbances. This issue has triggered numbers of research works in providing faster and continuous inertial support during any disturbances. Currently, the existing VIS can be categorized into two sections, namely, Rotating mass/Kinetic Energy (KE) stored in Wind Turbine (WT)'s rotor, and Energy storage [3–6]. In UK, the frequency delivered to consumers must be within ±1 % of its nominal value. Thus, to meet this requirement, all the generators connected to England and Wales's networks must have the technical capability to contribute to frequency control [7]. Besides, in between years of 2013/14 to 2033/34, the UK expected a reduction of inertial constant of up to 70 % if the conventional generators in the whole power system are

* Corresponding author at: Communication and Network Research Group, Malaysia-Japan International Institute of Technology, Universiti Teknologi Malaysia, 54100 Kuala Lumpur, Malaysia.
E-mail address: norshahida.kl@utm.my (N.S. Hasan).

https://doi.org/10.1016/j.est.2022.105181
Received 1 March 2022; Received in revised form 17 June 2022; Accepted 18 June 2022
Available online 4 July 2022

replaced with RESs [8,9].

1.2. Motivation of existing research works

Technically, WT possesses a certain amount of KE stored in its rotor which can be converted into inertial support using droop control technique [10,11], deloading technique [12,13] and inertia response technique [14]. These techniques are well known among researchers because no additional devices are required to supply the designated VIS. The droop control technique is designed to handle power imbalance between the input mechanical power and output electrical power of a wind turbine. However, this technique limits its applicability for a modern power system, namely, poor transient performance, ignoring load dynamics, poor performance in distribution network and inability to impose a fixed system frequency [15]. Meanwhile, the de loading technique enforces wind turbine to reserve enough power to fulfil the power imbalance. However, this deloading technique may increase the mechanical stress of the rotor which leads to the reduction of WT's lifetime and efficiency [16]. Thus, in order to achieve rapid and continuous VIS while avoiding any mechanical stress on the WT, this research proposed an improved VIS-based Hybrid Energy Storage (HES). According to [17–19], single energy storage is most unlikely to own both characteristics, thus hybrid energy storage formation is required to fulfil both requirements.

Here, the HES is composed of supercapacitor, (SC) and battery energy storage, (BES). The BES has low power density, high energy density, low self-discharge, low life cycle, long charge times, higher cost per watt and significantly lower cost per-watt hour. Meanwhile, the SC has high power density, low energy density, high self-discharge, high life cycle, short charge time, lower cost per watt and high cost per-watt hour [18,20–22]. Therefore, based on all these mentioned characteristics owned by BES and SC, these two ESSs offer complementary properties in meeting the main objective of this paper, which is, fast and continuous VIS.

Authors in [23] have implemented supercapacitor-based VIS in handling sudden loads increase and decrease. However, due to the high installation cost of a supercapacitor, this energy storage is unlikely able to provide long term inertial support during disturbances. Meanwhile, in 2021, Bera et al. proposed a novel analytical approach to size the energy storage systems in estimating the suitable inertial support to maintain the frequency stability of power grids [24]. Nevertheless, there is no clear declaration on which energy storages are employed. In [25], the inertia response is supplied by an ultra-capacitor (UC) while the battery energy storage in charge on damping control. Since the UC is directly connected to the DC bus, the variation in DC link voltage limits the inertia support from the UC due to modulation constraints. Additionally, the proposed HESS in [19] is controlled by a virtual energy storage technique where its parameters is optimized using particle swarm optimization technique and integral time absolute error. This proposed technique successfully improves the frequency nadir and ROCOF for all tested systems. However, the involvement of optimization techniques in obtaining the parameter values will significantly increase the simulation time and is not quite suitable for laege-scale system.

On the other hand, EMS is another crucial element in controlling the HES to ensure a better performance of HES in serving the required VIS. Shen *et. al* [26] presents a supervisory EMS for SC and BES to prolong the battery lifetime and achieve high-efficiency operation of HES. The Dynamic programming (DP) and Neural network (NN) is employed in this analysis to solve the mentioned optimization problem and split the generation from BES and SC respectively. However, the implementation of DP requires initial global information which is most unlikely suitable for a real-time management process. A model predictive control approach is proposed in [27] to ensure the HES operates within the specified operating constraints. Meanwhile, with the aim to achieve low computational cost and meet real time control requirements, Liu Chang *et. al* in [28] proposed a load adaptive parameter adjusting method to split the HES power based on load statistic. Nonetheless, these methods require heavy computation time due to their complex structure which might affect the response time and EMS procedure [29]. Hence it is recommended to solve all these issues.

1.3. Contribution of current research

Prior to the recommendation, this paper proposed a modified EMS which prioritized the involvement of SC in supplying the VIS before the BES gets into the network to pursue VIS procedure. To be brief, the proposed EMS offered a trade-off solution between SC and BES utilization while providing VIS to wind turbine system during frequency disturbances. Additionally, the contributions of the developed model are summarized as follows:

i. An improved mathematical formulation of SC and BES to mimic the behaviour of conventional SG in providing VIS during disturbances is introduced. The formulation is also based on the power mismatch between the mechanical input power and the electrical output power of the wind system.
ii. A modified EMS with reduced computational time of HES-based VIS to rapidly respond to the disturbances is implemented.
iii. An applicable HES-based VIS model with various range of test cases for validation has been developed.

1.4. Layout of the paper

This paper is organized as follows: Section 2 presents the system modelling that will be used to investigate the effectiveness of the proposed research work towards the applied disturbances. The derivations of proposed improved technique of HES-based VIS and modified EMS are carried out in Section 3. The related simulation results from the series tests are discussed in Section 4. The conclusions are drawn in Section 5.

2. System configuration and modelling

2.1. WECS and HES-based VIS modelling

Based on the previous research works on VIS, HES and wind turbine system, the WECS and proposed HES-based VIS is illustrated in Fig. 1. This model is composed of WT based permanent magnet synchronous generator (PMSG), DC-AC-DC converter, two separate Non-Isolated Bidirectional DCDC (NBDC) converters and loads. This model has been designed using MATLAB/Simulink simulation environment.

From this figure, it shows that, power that reaches the loads come from WT (P_{E_WT}), SG (P_{SG}) and HES (P_{sc} *and* P_{batt}). The power flows from SG and WT are regulated by HES via two separate NBDC converters. These two converters are controlled to complementarily charge and discharge the SC and BES based on the proposed modified EMS. The L1 and L2 are the fixed loads with values of 10 MW + 1MVAR and additional loads of 2 MW + 2MVAR respectively. The additional load acts as a sudden load increase (which enters the network during the second of 40) and decreases (leaves the network during the second of 70).

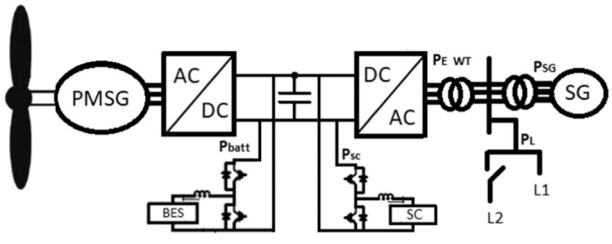

Fig. 1. WECS with the proposed HES-based VIS.

According to Fig. 1, the relationship between the electrical power of WT, P_{E_WT}, synchronous generator power, P_{SG}, power exchange between SC and the network, P_{SC}, power exchange between BES and the network, P_{batt} and load power P_L can be expressed as in Eq. (1). The ± defines the charge (+) and discharge mode (−) of SC and BES. Further mathematical formulations will be discussed in Section 3. The parameters involved in modelling the WECS and HES-based VIS in Fig. 1 are listed in Table 1 and can be found in Appendix A.

$$P_{E\_WT} + P_{SG} - P_L \pm P_{sc} \pm P_{batt} = 0 \tag{1}$$

2.2. HES's voltage and inductor selection in NBDC

Here, the NBDC is operated in continuous current mode (CCM) where the Inductor, L in Fig. 1 is the most crucial element to ensure the NBDC is operated in CCM instead of discontinuous current mode, (DCM). The size of the inductor can be significantly reduced by increasing the value of switching frequency. Therefore, the inductor is designed based on the CCM working mode and the demand of the current ripple, Δi_L during buck and boost mode. Since these two modes share the same inductor during their operating mode, therefore the inductance value must be properly designed. In [30], minimum inductance for buck, $L_{\min\_buck}$ and boost, $L_{\min\_boost}$ converters are expressed in two separate equations as in Eqs. (2) and (4). The duty cycle for each converter is expressed as in Eqs. (3) and (5) respectively. Subsequently, according to [30], in order to avoid discontinuous current mode, the value of inductance must be 25 % greater than its minimum value.

Sequentially, from [31], the Δi_L is the maximum ripple current that can be handled by SC and is set to be 2A. By considering a similar value of Δi_L the inductance value for both buck and boost modes, the minimum inductances values for these separate converters are obtained as in Eqs. (2) and (4). respectively. Where v_{sc} is the nominal value of SC, f_s is the switching frequency (20 kHz), v_o is the output voltage of the NBDC (equivalent to DC link voltage, 1150 V) and D is the duty ratio during boost mode, which can be calculated using Eq. (5). According to [32], the maximum stored energy that can be extracted from SC occurs at a duty cycle of 0.5. For this reason, the duty cycle is set to be 0.5 and the voltage for SC and BES can be obtained using Eqs. (3) or (5) by setting the DC link voltage at 1150 V. Therefore, after adding 25 % into Eq. (2), the inductance value for BDC is equivalent to 7.2 mH.

$$L_{min\_buck} = \frac{v_o(1 - D_{buck})}{\Delta i_L f_s} \tag{2}$$

$$v_o = v_s D_{buck}, D_{buck} = 0.5 \tag{3}$$

$$L_{min\_boost} = \frac{v_{sc} D_{boost}}{\Delta i_L f_s} \tag{4}$$

$$v_o = \frac{v_s}{1 - D_{boost}}, D_{boost} = 0.5 \tag{5}$$

3. Mathematical formulation and control scheme of HES-based VIS

Previously, Hasan et al. [23] proposed a modified technique in operating the SC-based VIS towards disturbances. Therefore, by employing a similar derivation procedure, this paper extends the VIS concepts into HES to ensure continuous inertial support.

Previously, the VISs are mostly supplied by SGs which can be expressed as in Eq. (6) where H is the SG inertia constant, f is the system frequency and ΔP is the power difference between the input mechanical power and the output electrical power of SG.

$$2Hf\frac{df}{dt} = \Delta P \tag{6}$$

By considering the similar behaviour of the power difference between the input and output of SG, ΔP, Eq. (7) is equalized to Eq. (6) to obtain the rate of power exchange between SC and the network. Assume that the SC is discharged.

$$-P_{E_{WT}} - P_{SG} + P_L = P_{sc} \tag{7}$$

$$\Delta P = P_{sc} \tag{8}$$

By equating Eq. (6) with Eq. (8), the required SC power with respect to the change frequency during load disturbances is written as in Eq. (9). The power extracted from SC is expressed as in Eq. (10).

$$2Hf\frac{df}{dt} = P_{sc} \tag{9}$$

$$P_{sc} = i_{sc} v_{sc} = c_{sc} v_{sc} \frac{dv_{sc}}{dt} \tag{10}$$

By equating Eq. (10) with Eq. (6), the VIS extraction from SC can be represented as in Eq. (11).

$$c_{sc}\, v_{sc}\, \frac{dv_{sc}}{dt} = 2H_{sc} f \frac{df}{dt} \tag{11}$$

By integrating both sides, it will get

$$\frac{c_{SC}\left(v_{SC}^2 - v_{sc0}^2\right)}{2} = H_{SC}\left(f^2 - f_0^2\right) \tag{12}$$

Where v_{sc0} and f_0 is the nominal values for SC voltage and system frequency respectively. To obtain new reference value of SC voltage, $v_{sc0}{}^*$, Eq. (12) can be linearized around its equilibrium point, as in Eq. (13). Then, the control process in defining the amount of energy to be extracted from or into the SC for VIS is expressed as in Eq. (14). Next, by rearranging Eq. (13), the new reference voltage for SC, $v_{sc0}{}^*$ is obtained as in Eq. (16).

$$c_{sc} v_{sc0} \Delta v_{sc} = 2H_{sc} f_0 \Delta f \tag{13}$$

$$H_{sc} = \frac{K_{sc} c_{sc} v_{sc0}}{2f_0} \tag{14}$$

where $K_{sc,}$ is the control parameter in defining the amount of power exchange between SC and network. The K_{sc} is defined as in Eq. (15) and this value is obtained using Linear regression technique.

$$K_{sc} = \frac{\Delta v_{sc}}{\Delta f} \tag{15}$$

$$v_{sc}^* = K_{sc}\Delta f + v_{sc0} \tag{16}$$

where c_{sc} is the capacitance of SC.

Afterwards, upon obtaining the new SC voltage, the required current flow from or into the SC can be expressed as in Eq. (17), where, K_H and K_{droop} is the coefficient for inertial and droop control [6], while $\Delta f = f_0 - f$. The current from Eq. (17) will be converted into PWM to switch the NBDC converter either to charge or discharge the SC.

$$i_{sc} = \frac{K_H \frac{d\Delta f}{dt} + K_{droop}\Delta f}{v_{sc}^*} \tag{17}$$

Meanwhile, for BES, the power exchange which reflects the power balance between supply and load can be written as follows:

$$P_{E\_WT} + P_{SG} - P_L - P_{sc} = \pm P_{batt} \tag{18}$$

$$\Delta P = P_{batt} \tag{19}$$

Previously, the VISs are mostly supplied by SGs and theirs behaviour can be expressed as in Eq. (20) [33]. Where H is the SG inertia constant, f is the system frequency and ΔP is the power difference between input mechanical power and the output electrical power of SG.

$$2Hf\frac{df}{dt} = \Delta P \tag{20}$$

Therefore, by equating Eq. (19) with Eq. (20), the required inertia support from BES with respect to the change of the frequency is obtained as in Eq. (21).

$$2Hf\frac{df}{dt} = P_{batt} \tag{21}$$

Integrating both sides of Eq. (21) with respect to time. Where E_{batt} in Eq. (24) is the energy provided by the BES when subjected to the disturbances. Let the initial state of energy of BES, E_{batt_0} is equal to zero.

$$\int_{f_0}^{f} 2Hf\, df = \int_{t_0}^{t} P_{batt} dt \tag{22}$$

$$H\left(f^2 - f_0^2\right) = P_{batt}(t - t_0) \tag{23}$$

$$E_{batt} - E_{batt\_0} = H\left(f^2 - f_0^2\right) \tag{24}$$

By assuming the small changes of the system states during system dynamics, Eq. (24) is linearized to its initial operating point and transforms into Eq. (25). The inertia time constant from BES, H_{batt} is obtained as in Eq. (26).

$$E_{batt} = 2H_{batt} f_0 \Delta f \tag{25}$$

$$H_{batt} = \frac{E_{batt}}{2f_0\Delta f} \tag{26}$$

The reference value of battery's current, i_{batt}* to be extracted or absorbed by BES during the disturbances is directly obtained by rearranging the ($P_{batt} = I_{batt} v_{batt}$) and is expressed as in Eq. (27).

$$i_{batt}^{*} = \frac{P_{batt}}{v_{batt}} \tag{27}$$

From Eqs. (14) and (26), it is concluded that the total available inertial time constant for HES-based VIS, H_{HES} can be expressed in Eq. (28). The first part is from SC and the other one is from BES.

$$H_{HES} = \frac{K_{sc} c_{sc} v_{sc0}}{2f_0} + \frac{E_{batt}}{2f_0\Delta f} \tag{28}$$

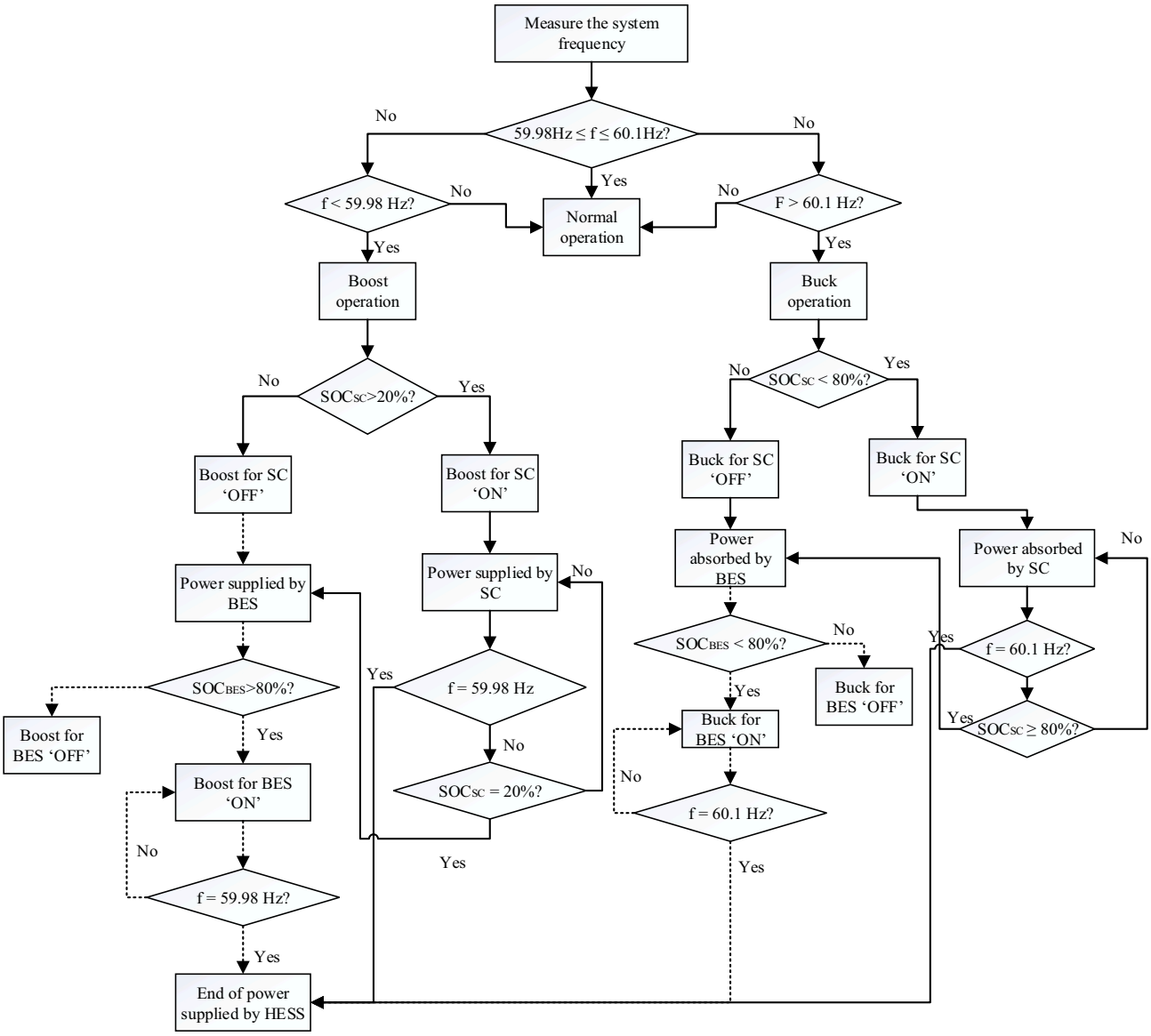

Fig. 2. Proposed EMS for HES-based VIS.

4. Proposed modified EMS

For smoother performance in handling large tested systems, this paper proposed a modified EMS by operating the SC until it reaches its minimum or maximum state of charge (SOC) during a power disturbance before the BES gets into the network to pursue the VIS process. In this way, the SC will be successfully utilized to provide the VIS and the charging and discharging process of the BES will be greatly be reduced. This reduction may prolong the life cycle of a BES.

Fig. 2 presents the proposed EMS of this study. First, the system frequency is measured at SG. If the measured system frequency is <59.98 Hz and the SOC of SC is more than its minimum set point (>20 %), the boost mode of SC will be 'ON' to discharge its stored energy to the DC link. If the SC reaches its minimum value, but the system frequency still has not regained its nominal value, then the BES will be discharged. At this particular time frame, the minimum SOC of SC is set to be 20 % so that the BES will enter the network a bit early to cope with its low power density. Conversely, if the measured system frequency goes >60.1 Hz, and the SOC of SC is <80 %, the buck mode of SC will be 'ON' to absorb part of the WT power to merge with the load decrement. As in the previous disturbance, if the maximum SOC of SC is reached, and the system frequency still has not reached its nominal value, the buck mode of BES will be 'ON' to pursue the power absorption from WT. At this time, the maximum SOC of SC is set to be 80 % to avoid deep discharge of SC.

5. Simulation results and discussion

This section investigates the effectiveness of the proposed HES-based VIS and modified EMS in handling load disturbances which enter (act as sudden load increases) and leave (act as sudden load decreases) the network at second of 40 and 70 accordingly. Here, in order to analyse the effectiveness of the proposed research work towards different wind penetration levels, two WT sizes of 3 MW and 6 MW will be considered. Meanwhile, the SG is kept at 10MVA. The fixed load is set to be 10 MW + 1MVAR while the additional loads that enter and leave the network are set to be 2 MW and 0.2MVAR respectively. There are three series tests that will conducted in this section:

i. Fixed wind speed with fluctuated loads for both wind penetration levels.
ii. Variable wind speed condition with fixed load for the 6 MW WT system.
iii. Variable wind speed with fluctuated loads for the 6 MW WT system.

5.1. Fixed wind speed with fluctuated loads for both wind penetration levels

This section validates the proposed HES-based VIS with three other scenarios, namely, without any VIS, with SC-based VIS and BES based VIS under fixed wind speed and fluctuated load disturbances. The SC-based VIS and BES-based VIS are denoted as the sole ES of SC and BES that act as VIS throughout the simulation time. This analysis aims to prove the aforementioned claim of the proposed HES-based VIS which is able to provide faster and limitless VIS throughout the disturbances. The 2 MW + 0.2 MVAR load suddenly steps in and out of the network during the second of 40 and 70 respectively. The input wind speed is fixed at 12 m/s.

5.1.1. For 3 MW WT system

Here, the WT is set to be 3 MW. The obtained simulation results, which consisted of system frequency, WT conversion power, SG power, SOC of SC and BES are presented in Fig. 3(a–e) accordingly. From Fig. 3 (a), scenarios (2) and (4) shared identical behaviour in their frequency

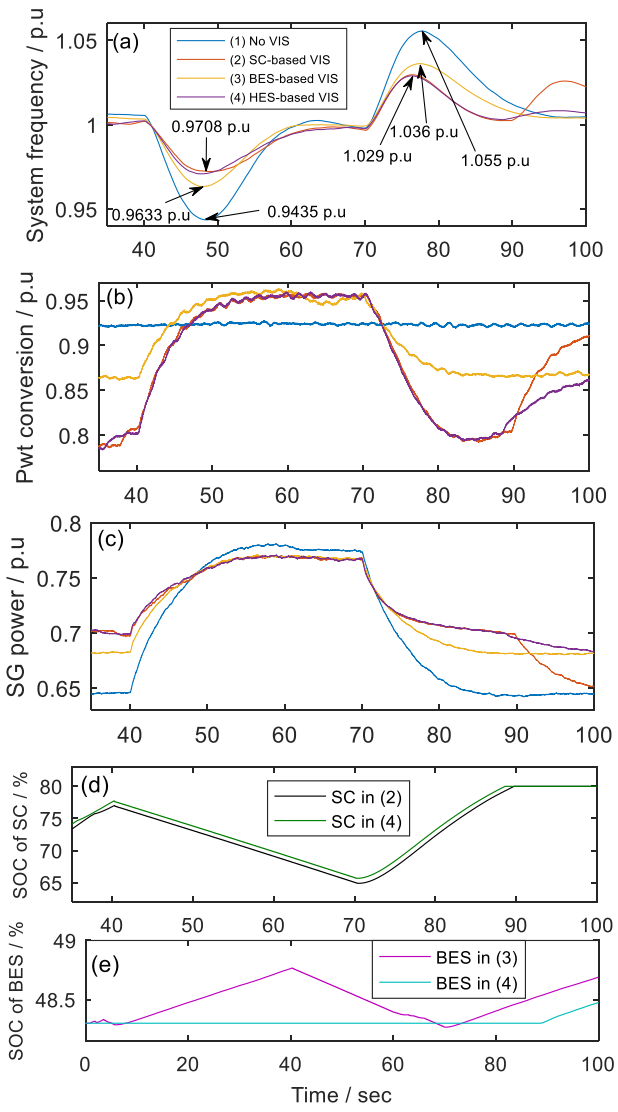

Fig. 3. Simulation results of (a) System frequency, (b) Pwt conversion (c) SG power, (d) SOC of SC and (e) SOC of BES for 3 MW WT system.

nadir improvements and peak frequency reductions. This is because, the proposed EMS in this paper prioritizes the SC operation until it reaches its maximum or minimum SOC, therefore in this case, as the SC still varies within 20 % and 80 % SOC, thus, in these two cases, the SC alone is enough to provide the required VIS during frequency nadir and peak frequency response improvement. Therefore, from Fig. 3(a), the SC (in scenario (2) and (4)) significantly improves the frequency nadir and peak frequency from 0.9435 p.u to 0.9708 p.u (approximately 2.9 % improvement) and 1.05 p.u to 1.02 p.u (approximately 2.46 % reduction) correspondingly. Meanwhile, the BES in scenario (3) is only able to provide the respective improvement and reduction by 2.1 % and 1.8 %. It can be noted here that, the slow dynamic behaviour of BES is unlikely to be able to provide rapid VIS to improve the frequency nadir and peak frequency during disturbances compared to SC.

Throughout scenarios (2–4), the SC and BES significantly regulate the power extraction from WT (Fig. 4.3(b)) and SG (Fig. 4.3(c)) by actively charging and discharging its stored power based on designated EMS and their dynamic response behaviours to regain the stability of system frequency. However, the SC alone in scenario (2) failed to maintain the stability of system frequency after the second of 91 (as in Fig. 3(a)). This is due to the excess power from WT that needs to continuously be absorbed by SC, yet the SC already reached its

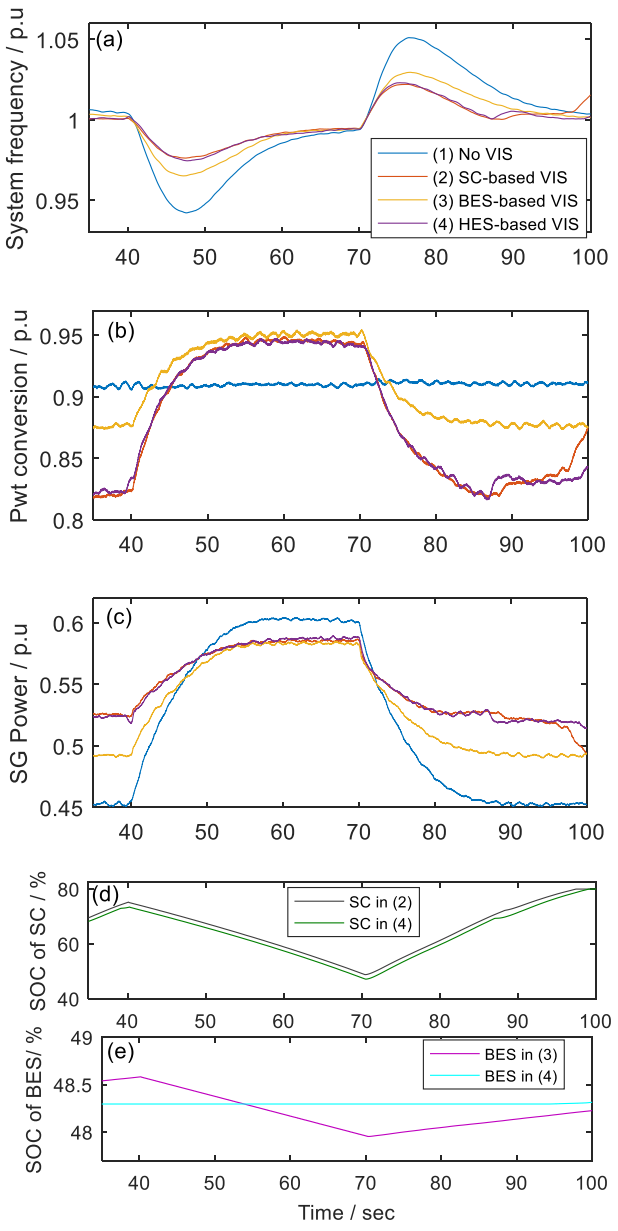

Fig. 4. Simulation results of (a) System frequency, (b) Pwt conversion (c) SG power, (d) SOC of SC and (e) SOC of BES for 6 MW WT system.

maximum SOC (as in Fig. 3(d)). Consequently, at this time, this excess power abused the stability of the system frequency signal during the last 9 s. Conversely, with the proposed research works (in scenario (4)), the system frequency signal during the last 9 s in Fig. 3(a) remains at its nominal value as the BES (scenario (4) in Fig. 3(e)) continues to absorb the excess power from the network. Therefore, it can be concluded here that, the proposed research works in this paper are not only able to provide highest improvement in terms of frequency nadir and peak frequency during sudden load increase and decreases respectively, but also able to maintain the system frequency's stability during certain time interval which failed to be done by SC alone.

5.1.2. For 6 MW WT system

This section further validates the proposed HES-VIS towards larger WT size, 6 MW. Similar load disturbances are applied here. The obtained simulation results are illustrated in Fig. 4(a–e). From Fig. 4(a) until (c), the SC (in scenario (2) and (4)) once again proved its fast response behaviour to regulate the WT conversion power (Fig. 4(b)) and SG power (Fig. 4(c)) to respond to the load disturbances. These regulations slow down the decrement and increment of frequency nadir and peak frequency by 3.5 % and 2.7 % respectively. The effects of frequency nadir and peak frequency for all the aforementioned scenarios are represented in Tables 1 and 2 accordingly.

In comparison with the smaller WT size, 3 MW (in Section 5.1.1), larger WT size successfully reduces the SG power generation to serve the designated load. This reduction significantly reduces the involvement of conventional generators which is normally operated by hydraulic, steam, diesel, fossil fuel and any other high carbon emission turbine. These occurrences further reduce CO2 emissions while encouraging higher wind penetration levels to be integrated to the electrical network. Additionally, the integration of HES-based VIS promises stability performance of system frequency signals in handling disturbances.

5.1.3. Frequency nadir and peak frequency variation for 3 MW and 6 MW WT systems

The Tables 2 and 3 summarize the variation on frequency nadir and peak frequency for both WT systems. Tables 2 and 3 can be found in Appendix B. From Table 2, it can be noted here that, with no VIS, system frequency in 6 MW WT system produced slightly lower frequency nadir, 0.9424p.u compared to 3 MW WT system, with 0.9435p.u. However, its frequency nadir improvement is 3.5 %, which is higher than the 3 MW WT system, 2.8 %. This is because, in 6 MW WT system, the available wind power to serve the load is higher compared to 3 MW WT system, thus, during the sudden load that increased at second of 40, the SC efficiently slowed down the rate of change of frequency and making the frequency nadir to reach its minimum value only at 9.764p.u. Similar response behaviour for 6 MW WT system can be seen during sudden load decreases (as in Table 3) where the SC in scenario (2) and (4) successfully slowed down the increment of peak frequency and made the peak frequency to reach its maximum point at 1.023p.u, equivalent to 2.7 % decrement. This percentage of decrement is higher compared to the 3 MW WT system, 2.5 %.

5.2. Variable wind speed with fixed load for 6 MW WT system

Subsequently, to further investigate the feasibility of the proposed research works in providing faster and continuous VIS response towards disturbances, this section extends the simulation test under variable wind conditions at constant load behaviour using only 6 MW WT system. The 3 MW WT is not considered in this analysis because the previous section had proved that the proposed HES-based VIS provides significant improvement in 6 MW WT compared to 3 MW WT. The variation of wind speeds is randomly varied within a 2 s interval, as in Fig. 5. Here, the WT and SG are kept at 6 MW and 10 MVA respectively, while the load is fixed at 10 MW + 1MVAR. Since the previous subsection proved the delayed dynamic behaviour of SC, BES and HES in responding to the sudden load increases and decrease, therefore only two scenarios will be carried out here, which is, (1) no VIS and (2) proposed HES-based VIS.

The simulation results for this test are illustrated in Fig. 6(a–e). From Fig. 6(a), the system frequency with the proposed HES-based VIS varies

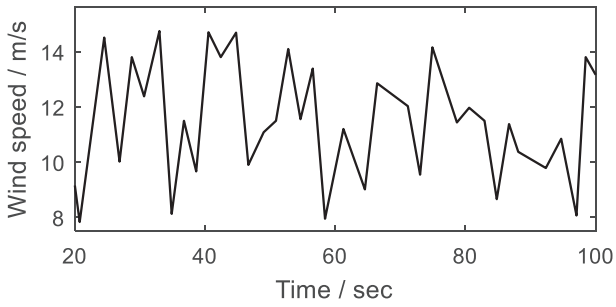

Fig. 5. Variable wind speed pattern.

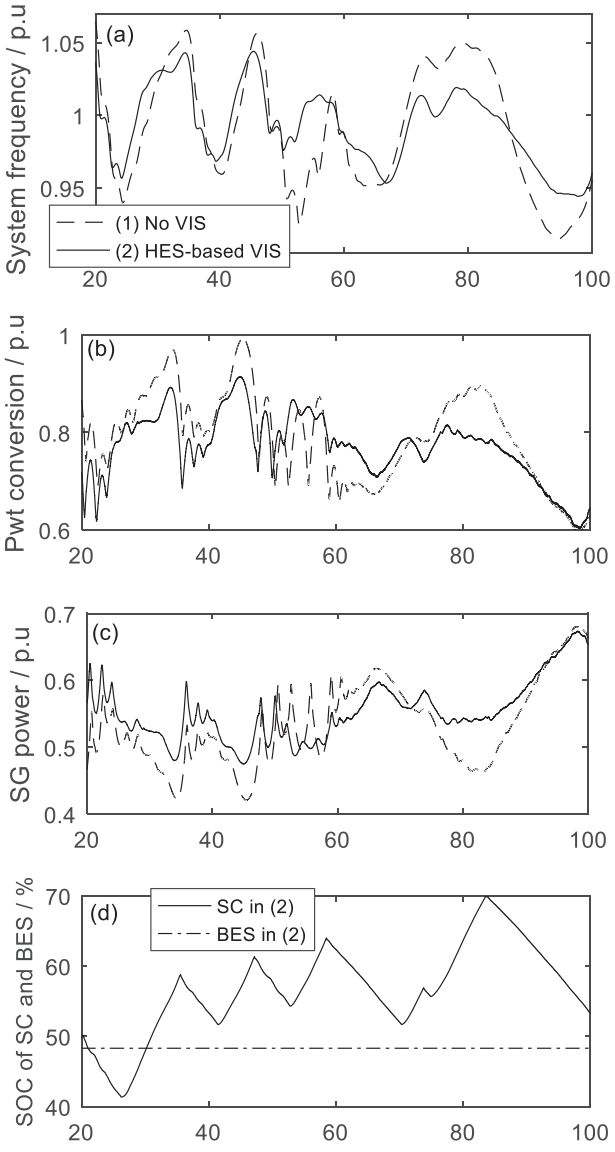

Fig. 6. Simulation results of (a) System frequency, (b) WT conversion power, (c) SG power (d) SOC of SC and BES.

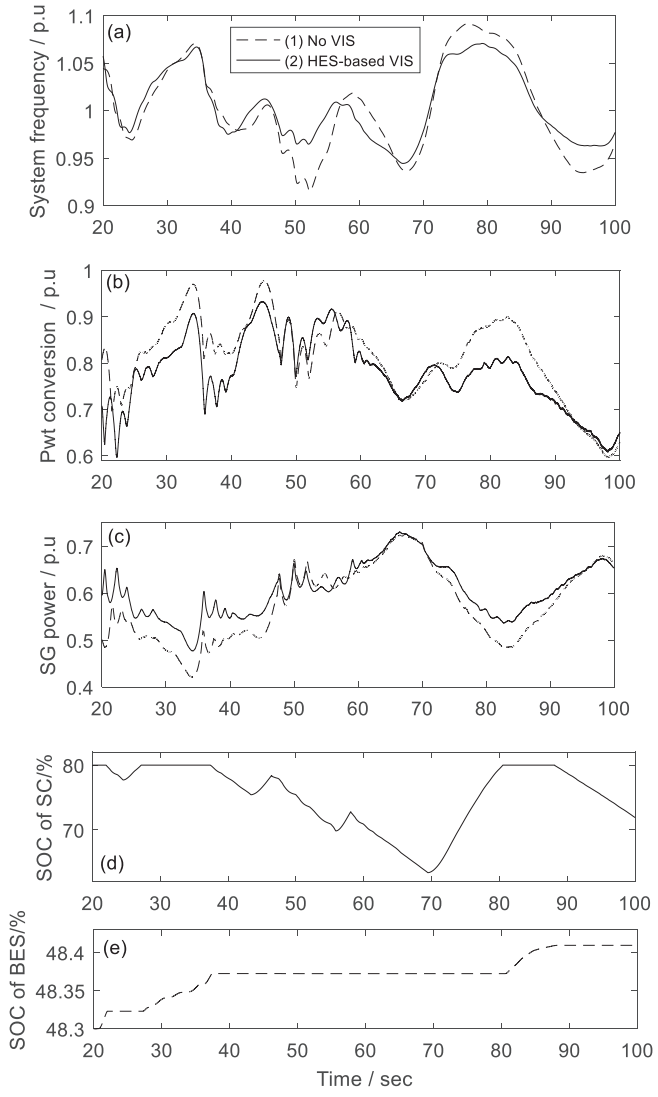

Fig. 7. Simulation results of (a) System frequency, (b) WT conversion power, (c) SG power (d) SOC of SC and (e) SOC of BES.

in smaller range and more stable compared to the one without the presence of VIS. As the HES is actively charged and discharged to restore the system frequency stability, the WT conversion power (Fig. 6(b)) follows the trend of the proposed EMS towards HES. At this time, the SG regulates its generation power to compensate for the load gap and can be seen in Fig. 6(c). Throughout Fig. 5(a–e), It can be observed here that the SC in the proposed HES-based VIS greatly slowed down the variation response of the system frequency by actively charging and discharging its stored energy to and from the network respectively. Meanwhile, the proposed EMS in this paper makes the BES (Fig. 6(e)) remains at its constant SOC as the SC did not reach its maximum or minimum SOC. This occurrence significantly prolongs the life cycle of the BES itself.

5.3. *Variable wind speed with variable load for 6 MW WT system*

Likewise, in this section, the proposed research works is further evaluated under variable speed wind conditions and variable load disturbances. Similar load disturbances as in Section 5.1 are employed here, where the 2 MW + 2MVAR enters and leaves the network at second of 40 and 70 respectively. The simulation results from this test are illustrated in Fig. 7(a–e). Throughout the disturbances from fluctuated wind speed and loads, it can be concluded that the proposed research works in this paper greatly slows down the frequency response (Fig. 7 (a)) by complementarily charging and discharging the stored energy of SC and BES (Fig. 7(d–e)). Consequently, the WT conversion power (Fig. 7(b)) and SG power (Fig. 7(c)) are regulated to bridge the gap between supply and demand. The proposed HES-based VIS greatly reduces the operating range of SG which may lead to the increment of SG reliability in serving the load. From Fig. 7(d) and (e), it shows that, within certain time intervals, where the SC reaches its maximum of SOC, 80 %, the BES successfully gets into the network to pursue the VIS process by absorbing part of the WT power to reduce the power imbalance in the network.

6. Conclusion

This paper proposed and investigated the feasibility of an improved technique in translating the HES into VIS and modified the EMS of HES towards disturbances. This research work aims to provide faster and continuous inertial support throughout disturbances while prolonging the lifetime of BES. From the series simulation tests in Section 5, it can be seen that the proposed research works in this paper significantly improves the frequency nadir and peak frequency while maintaining the stability of the system frequency compared to SC-based VIS and BES-

based VIS. The low power density behaviours of BES show delayed dynamic response towards the applied disturbances compared to SC. Therefore, the proposed EMS of prioritizing the SC until it reaches the maximum or minimum SOC before the BES gets into the network promises faster VIS under a certain time interval while prolonging the lifetime of BES itself. In addition, for the tested systems in this paper, it can be concluded that, larger WT size provides higher frequency nadir and peak frequency improvement compared to the smaller one. However, the maximum size of WT and load that can be handled by the proposed HES-based VIS is not covered in this paper.

Funding information

The authors would like to thank the Ministry of Higher Education of Malaysia for the financial funding of this project under Q. J130000.3551.06G65, the Research Management Centre (RMC) of Universiti Teknologi Malaysia, Centre of Electrical Energy Systems (CEES), School of Electrical Engineering, UTM, UTM for their support for the research management.

CRediT authorship contribution statement

Nor Shahida Hasan has conducted the experiment and write the original article. Norzanah Rosmin, Norjulia Mohamad Nordin, and Saifulnizam Abd Bakar have edited the text and review the manuscript. Norzanah Rosmin, Norjulia Mohamad Nordin, and Saifulnizam Abd Bakar have proofing the manuscript. All authors reviewed the manuscript.

Declaration of competing interest

The authors declare that they have no known competing financial interests or personal relationships that could have appeared to influence the work reported in this paper.

Appendix A

Table 1
Parameters for Wind PMSG [6,33,34].

	Item	Value
Wind PMSG	Rated wind speed	12 m/s
	PMSG rated power, voltage, frequency	3 MW and 6 MW, 575 V, 50 Hz
	Rated rotor speed	1.23p.u
	Inertia constant, H_g	1.15 s
	Stator resistance (Rs), inductances (L_d, L_q)	50μΩ, 0.0055H, 0.00375H
	Number of pole pairs, (p)	11
Converters	Resistance and Inductance of grid side	R = 0.003p.u, L = 0.3 p.u
	DC-link capacitor and voltage	9000 μF, 1.15 kV
SG	Rated MVA, terminal voltage, Frequency	10MVA, 6.6 kV, 60 Hz
	Inertia time constant	4 s
	d-axis synchronous reactance (x_d, x_d', x_d")	1.305, 0.296, 0.252
	q-axis synchronous reactance (x_q, x_q", x_l)	0.474, 0.243, 0.18
	SG time constant (T_d', T_d", T_q")	1.01, 0.053, 0.1

Appendix B

Table 2
Frequency nadir improvement.

WT size	No VIS/p.u	SC-based VIS/p.u	BES-based VIS/p.u	HES-based VIS/p.u
3 MW	0.9435	0.9708 (2.8 % improvement)	0.9633 (2.1 % improvement)	0.9708 (2.8 % improvement)
6 MW	0.9424	0.9764 (3.5 % improvement)	0.9653 (2.4 % improvement)	0.9764 (3.5 % improvement)

Table 3
Peak frequency decrement.

WT size	No VIS/p.u	SC-based VIS/p.u	BES-based VIS/p.u	HES-based VIS/p.u
3 MW	1.055	1.029 (2.5 % decrement)	1.036 (1.8 % decrement)	1.029 (2.5 % decrement)
6 MW	1.051	1.023 (2.7 % decrement)	1.029 (2.1 % decrement)	1.023 (2.7 % decrement)

References

[1] I. Irena, Future of Wind: Deployment, Investment, Technology, Grid Integration and Socio-economic Aspects, 2019.
[2] I.M. Sanz, B. Chaudhuri, G. Strbac, Inertial response from offshore wind farms connected through DC grids, IEEE Trans. Power Syst. 30 (3) (2014) 1518–1527.
[3] N. Mendis, et al., Hydrogen energy storage for a permanent magnet wind turbine generator based autonomous hybrid power system, in: 2011 IEEE Power and Energy Society General Meeting, IEEE, Detroit, MI, USA, USA, 2011.
[4] H. Silva-Saravia, H. Pulgar-Painemal, J.M. Mauricio, Flywheel energy storage model, control and location for improving stability: the Chilean case, IEEE Trans. Power Syst. 32 (4) (2016) 3111–3119.

[5] G. Delille, B. Francois, G. Malarange, Dynamic frequency control support by energy storage to reduce the impact of wind and solar generation on isolated power system's inertia, IEEE Trans.Sustain.Energy 3 (4) (2012) 931–939.
[6] Y. Tan, et al., Enhanced frequency response strategy for PMSG based wind energy conversion system using ultracapacitor in remote area power supply systems, IEEE Trans. Ind. Appl. 53 (1) (2016) 549–558.
[7] I. Erinmez, et al., NGC experience with frequency control in England and Wales-provision of frequency response by generators, in: Power Engineering Society 1999 Winter Meeting, IEEE, IEEE, New York, NY, USA, 1999.
[8] J. Leslie, Electricity Ten Year Statement (ETYS) 2017- UK Electricity Transmission, National Grid ESO, 2017.
[9] M. Dreidy, H. Mokhlis, S. Mekhilef, Inertia response and frequency control techniques for renewable energy sources: a review, Renew. Sust. Energ. Rev. 69 (2017) 144–155.
[10] K.M. Abo-Al-Ez, R. Tzoneva, Active power control (APC) of PMSG wind farm using emulated inertia and droop control, in: 2016 International Conference on the Industrial and Commercial Use of Energy (ICUE), IEEE, Cape Town, South Africa, 2016.
[11] J. Van de Vyver, et al., Droop control as an alternative inertial response strategy for the synthetic inertia on wind turbines, IEEE Trans. Power Syst. 31 (2) (2016) 1129–1138.
[12] Z. Wu, et al., Coordinated control strategy of battery energy storage system and PMSG-WTG to enhance system frequency regulation capability, IEEE Trans. Sustain.Energy 8 (3) (2017) 1330–1343.
[13] Y. Wang, et al., Control of PMSG-based wind turbines for system inertial response and power oscillation damping, IEEE Trans.Sustain.Energy 6 (2) (2015) 565–574.
[14] B. Singh, S. Sharma, Stand-alone wind energy conversion system with an asynchronous generator, J.Power Electron. 10 (5) (2010) 538–547.
[15] M. Yazdanian, A. Mehrizi-Sani, Distributed control techniques in microgrids, IEEE Trans.Smart Grid 5 (6) (2014) 2901–2909.
[16] X. Qi, et al., Tracking-differentiator-based dynamic virtual inertial control of offshore wind power plant for frequency regulation, Int. J. Electr. Power Energy Syst. 141 (2022), 108150.
[17] N.S. Hasan, et al., Review of storage schemes for wind energy systems, Renew. Sust. Energ. Rev. 21 (2013) 237–247.
[18] U. Akram, M. Khalid, A coordinated frequency regulation framework based on hybrid battery-ultracapacitor energy storage technologies, IEEE Access 6 (2018) 7310–7320.
[19] M.M. Mohamed, et al., Optimal virtual synchronous generator control of battery/supercapacitor hybrid energy storage system for frequency response enhancement of photovoltaic/diesel microgrid, J.Energy Storage 51 (2022), 104317.
[20] Q. Xu, et al., A decentralized dynamic power sharing strategy for hybrid energy storage system in autonomous DC microgrid, IEEE Trans. Ind. Electron. 64 (7) (2016) 5930–5941.
[21] M. Daoud, M. Ghorbel, H. Mnif, A power control approach for a biosensor battery-supercapacitor storage system, J.Energy Storage 43 (2021), 103166.
[22] M.C. Argyrou, et al., A novel power management algorithm for a residential grid-connected PV system with battery-supercapacitor storage for increased self-consumption and self-sufficiency, Energy Convers. Manag. 246 (2021), 114671.
[23] N.S. Hasan, et al., Virtual inertial support extraction using a super-capacitor for a wind-PMSG application, IET Renew.Power Gener. 13 (10) (2019) 1802–1808.
[24] A. Bera, B. Chalamala, R.H. Byrne, J. Mitra, Sizing of energy storage for grid inertial support in presence of renewable energy, in: IEEE Transactions on Power Systems, 2021, https://doi.org/10.1109/TPWRS.2021.3134631.
[25] J. Fang, et al., A battery/ultracapacitor hybrid energy storage system for implementing the power management of virtual synchronous generators, IEEE Trans. Power Electron. 33 (4) (2017) 2820–2824.
[26] J. Shen, A. Khaligh, A supervisory energy management control strategy in a battery/ultracapacitor hybrid energy storage system, IEEE Trans.Transport. Electrification 1 (3) (2015) 223–231.
[27] B. Hredzak, V.G. Agelidis, M. Jang, A model predictive control system for a hybrid battery-ultracapacitor power source, IEEE Trans. Power Electron. 29 (3) (2014) 1469–1479.
[28] C. Liu, et al., Load-adaptive real-time energy management strategy for battery/ultracapacitor hybrid energy storage system using dynamic programming optimization, J. Power Sources 438 (2019), 227024.
[29] S. Dusmez, A. Khaligh, A supervisory power-splitting approach for a new ultracapacitor–battery vehicle deploying two propulsion machines, IEEE Trans.Ind. Inform. 10 (3) (2014) 1960–1971.
[30] D.W. Hart, Power Electronics, McGraw-Hill, New York, 2011.
[31] J. Leuchter, et al., Bi-directional DC-DC converters for supercapacitor based energy buffer for electrical gen-sets, in: 2007 European Conference on Power Electronics and Applications, IEEE, Aalborg, Denmark, 2007.
[32] Ned Mohan, Tore M. Undeland, W.P. Robbins, 7.4 step-up boost converter, in: Power Electronics Converters, Applications and Design 2002, John Willey & Sons, Inc, 2003.
[33] Y. Li, Z. Xu, K.P. Wong, Advanced control strategies of PMSG-based wind turbines for system inertia support, IEEE Trans. Power Syst. 32 (4) (2017) 3027–3037.
[34] (Hydro-Quebec), R.G. Wind Farm - DFIG Detailed Model, cited 2020; Available from: https://ww2.mathworks.cn/help/physmod/sps/examples/wind-farm-dfig-detailed-model.html.

Update

Journal of Energy Storage

Volume 56, Issue PB, 10 December 2022, Page

DOI: https://doi.org/10.1016/j.est.2022.106141

Journal of Energy Storage 56 (2022) 106141

Contents lists available at ScienceDirect

Journal of Energy Storage

journal homepage: www.elsevier.com/locate/est

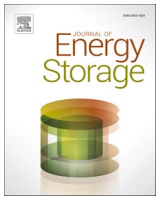

Corrigendum

Corrigendum to "Dynamic response of hybrid energy storage based virtual inertial support in wind application" [J. Energy Storage, 53 (2022) 105181]

Nor Shahida Hasan [a,b,*], Norzanah Rosmin [a,b], Norjulia Mohamad Nordin [c], Saifulnizam Abd Khalid [c], Azana Hafizah Mohd Aman [d]

[a] Communication and Network Research Group, Malaysia-Japan International Institute of Technology, Universiti Teknologi Malaysia, 54100 Kuala Lumpur, Malaysia
[b] Centre of Electrical Energy Systems (CEES), School of Electrical Engineering, Faculty of Engineering, Universiti Teknologi Malaysia, 81310 Johor Bahru, Johor, Malaysia
[c] School of Electrical Engineeting, Faculty of Engineering, Universiti Teknologi Malaysia, 81310 Johor Bahru, Johor, Malaysia
[d] Faculty of Information Science and Technology, Universiti Kebangsaan Malaysia, 43600 UKM Bangi, Selangor, Malaysia

The authors regret on the mistake in which one of the authors' names was overlooked. Saifulnizam Abd Bakar should allegedly be replaced with Saifulnizam Abd Khalid.

The authors would like to apologise for any inconvenience caused.

DOI of original article: https://doi.org/10.1016/j.est.2022.105181.

* Corresponding author at: Communication and Network Research Group, Malaysia-Japan International Institute of Technology, Universiti Teknologi Malaysia, 54100 Kuala Lumpur, Malaysia.

E-mail address: norshahida.kl@utm.my (N.S. Hasan).

https://doi.org/10.1016/j.est.2022.106141

Available online 17 November 2022
2352-152X/